

measurement of standard neutrino oscillation parameters, mainly facilitating tests of the anisotropic LIV mechanism by search for a time-varying neutrino oscillation, while the static anisotropic LIV effects received scant attention.

Current reactor neutrino oscillation experiments primarily focus on mixing angle θ_{13} and the effect mass squared difference Δm_{ee}^2 , represented by short-baseline reactor neutrino experiments, such as Double Chooz [41], RENO [42], and Daya Bay [43]. They nailed down the sub-percent precision on θ_{13} . However, the consistency between the the best-fit results from three reactor neutrino experiments in the standard neutrino oscillation picture demonstrates Parameter Goodness-of-fit [44] ($p_{PG} = 0.14$), residing the proximity to the tension boundary. It is a question whether the incompatibility points to new physics beyond three neutrino oscillations. For example, an anisotropy caused by the LIV mechanism could logically lead to a discrepancy, since neutrinos propagate in different directions for these reactor experiments. Then it deserves investigating the effects of anisotropic LIV on the analyses of θ_{13} and Δm_{31}^2 in the Double Chooz, RENO, and Daya Bay reactor neutrino experiments. This paper aims to further extend the study to anisotropic Lorentz invariance violating phenomena in reactor neutrino oscillation experiments, focusing on inherent directional differences rather than the traditional time-dependent sidereal effects.

The structure of the article is as follows: In Section 2, we briefly introduce the theoretical framework of anisotropic LIV. In Section 3, we describe the experimental data and numerical methods adopted in this work. Section 4 presents the impact of anisotropic LIV effects on the analysis of existing short-baseline reactor neutrino oscillation data. In the end, Section 5 gives the summary and conclusion.

2 Anisotropic Lorentz invariance violation in neutrino oscillation

We will briefly review the mathematical formulation of neutrino oscillation theory with LIV in this section and provide the effective expression for the survival probability of electron antineutrinos. The theoretical model originates from Ref. [45], while the simplification of effective parameter is similar to Ref. [46]. Since the mass of neutrinos is extremely small, smaller than 0.8 eV based on the latest KATRIN results [47], the LIV energy-momentum dispersion relation can be expressed under extreme relativistic approximation [48]:

$$E \simeq |\mathbf{p}| + \frac{m^2}{2|\mathbf{p}|} + \sum_{n=1}^{\infty} \gamma_{LIV,n} |\mathbf{p}|^{n-1}. \quad (1)$$

In Eq. (1), the second term on the right-handed side is a perturbative expansion of the neutrino mass term, and

the third term predicts subtle LIV suppressed by the Planck scale $E_{Pl} \simeq 10^{19}$ GeV [49]. Ignoring neutrino-antineutrino mixing, the LIV Lagrangian in the neutrino sector of SME is given by [50, 51]

$$\begin{aligned} \mathcal{L}_D = & -\bar{\nu}_\alpha (a^\mu \gamma_\mu + b^\mu \gamma_5 \gamma_\mu) \nu_\beta \\ & + \frac{i}{2} \bar{\nu}_\alpha (c^{\mu\nu} + d^{\mu\nu} \gamma_5) \gamma_\mu \overleftrightarrow{\partial}_\nu \nu_\beta. \end{aligned} \quad (2)$$

The subscripts $\alpha, \beta = e, \mu, \tau$ of the neutrino field correspond to different lepton flavors. If we assume that the mass eigenstates of neutrinos are the physical states propagating with LIV in vacuum, the effective Hamiltonian for neutrino oscillations in flavor eigenstates with LIV can be expressed as [52]

$$\mathcal{H}_{\nu\nu}^{\text{eff}} = U^\dagger \left(\frac{M^2}{2E} + \mathcal{H}_{LIV} \right) U + V_{\text{matter}}. \quad (3)$$

The unitary matrix U is the PMNS matrix [53], and V_{matter} is the matter potential term. After removing the LIV term, $(\mathcal{H}_{\nu\nu})_{\text{eff}}$ is the effective Hamiltonian for standard neutrino oscillations. In the leading-order perturbative expansion approximation, considering the Sun-centered reference frame with the Earth's rotation axis as the z -axis [46], the Hamiltonian term $\mathcal{H}_{LIV}^{\text{eff}} = \text{Diagonal}(0, \Delta\gamma_{21}, \Delta\gamma_{31})$ causing anisotropic LIV can be reconstructed into a form depending on directional factors,

$$\begin{aligned} \Delta\gamma_{ij} = & (\mathcal{A}_{ij}^{S(0)} + \mathcal{A}_{ij}^{S(1)} E) \sin \theta^{\text{LIV}} \\ & + (\mathcal{A}_{ij}^{C(0)} + \mathcal{A}_{ij}^{C(1)} E) \cos \theta^{\text{LIV}} \\ & + \mathcal{B}_{ij}^S E \sin(2\theta^{\text{LIV}}) + \mathcal{B}_{ij}^C E \cos(2\theta^{\text{LIV}}), \end{aligned} \quad (4)$$

where the \mathcal{A}, \mathcal{B} parameters are effective LIV coefficients in general form for a several year experiment. $\mathcal{A}^{(0)}$ would undergo a sign inversion by CPT transformation in the antineutrino case. The LIV correction term depends only on the polar angle θ^{LIV} in the direction. The relation between SME coefficients and effective anisotropic LIV parameters can be found in the Appendix A.

θ^{LIV} is the angle between the neutrino beam and the Earth's rotation axis, given by

$$\theta^{\text{LIV}} = \arccos(-\sin \chi \cos \phi), \quad (5)$$

as zenith angle approximates right angle for reactor neutrino experiments. χ is the co-latitude of the location of the detector, while ϕ is the angle between the neutrino beam and the south measured towards the east. $\cos \phi$ reflects the projection of the beam in the due south direction, which contributes to the axial component, as shown in Fig. 1. Since eastward or westward displacement does not alter this axial projection, θ^{LIV} does not change by the Earth's rotation without inducing a time-dependent sidereal effect.

The survival probability of reactor electron antineutrinos with anisotropic LIV in short-baseline reactor experiments

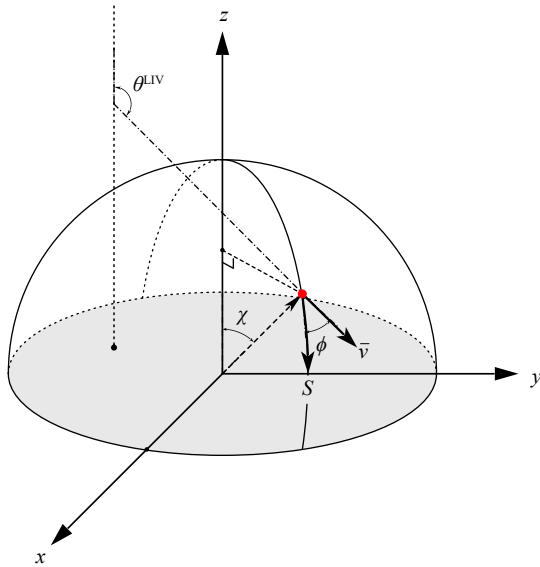


Fig. 1 The sketch to show how antineutrinos propagate along the Earth's surface. The silhouette of Earth's northern hemisphere is with the rotation axis as the z -axis. The red dot represents the geographical location of the detector, while the label "S" marks the due south at this point.

can be written as follows:

$$\begin{aligned}
 P_{\bar{\nu}_e \rightarrow \bar{\nu}_e} \approx & 1 - \sin^2(2\theta_{13}) \sin^2 \left[\left(\frac{\Delta m_{ee}^2}{4E} + \frac{\Delta \gamma_{31}}{2} \right) L \right] \\
 & - \cos^4 \theta_{13} \sin^2(2\theta_{12}) \sin^2 \left[\left(\frac{\Delta m_{21}^2}{4E} + \frac{\Delta \gamma_{21}}{2} \right) L \right].
 \end{aligned} \quad (6)$$

Here, $\Delta m_{ee}^2 = \cos^2 \theta_{12} \Delta m_{31}^2 + \sin^2 \theta_{12} \Delta m_{32}^2$.

In the LIV framework, neutrino oscillations acquire linear phase terms with energy dependence, which grow in magnitude with increasing energy in contrast to standard neutrino oscillation phases $\Delta m^2 L/E$, thereby allowing for a more flexible fit to the reconstructed neutrino energy spectrum. Moreover, θ^{LIV} in $\Delta \gamma$ depends on specific propagation direction, leading to LIV phase variations across different experiments and resulting in inconsistent survival probabilities even at identical energy and baseline. Thus, these subtle LIV-induced differences may help explain the discrepancies between the best-fit results of short-baseline reactor neutrino experiments when LIV effects are neglected.

3 Simulation details

In the present work, we focus on data analysis from short-baseline reactor experiments Double Chooz, RENO and Daya Bay. These experiments relied on large flux of $\bar{\nu}_e$ from reactors and detected $\bar{\nu}_e$ in liquid scintillator (LS) by inverse-beta-decay (IBD). Then the energy of $\bar{\nu}_e$ is inferred from a prompt-energy ($E_{\bar{\nu}} \sim E_{\text{prompt}} +$

0.78 MeV). Recent published data from Double Chooz, RENO, and Daya Bay [43, 54, 55] are reproduced within the GLOBES framework [56–59]. Main configuration for each experiment is shown in Table 1 [60].

Since the results from GLOBES are consistent with that from reference, we investigate the effects of anisotropic LIV on the measurements of θ_{13} and Δm_{ee}^2 . In this section, we briefly introduce the mock data preparations in each experiment and present the data analysis methods used in the study. Detailed computational procedures and their implementations can be accessed through the public GitHub repository [61].

3.1 Double Chooz experiment

The Double Chooz experiment made good use of Chooz reactors, which are located at Chooz in France with a co-latitude of $\chi = 39.9^\circ$, with total power of 8.5 GW_{th}. The near detector (ND) and the far detector (FD) are located approximately at 400 m and 1050 m from reactor cores, respectively. The far detector was put to the east of the reactors at an angle of $\phi = 63.4^\circ$, corresponding to $\theta^{\text{LIV}} = 1.86$ rad.

The core of the Double Chooz detector contained 10.3 m³ of LS with 0.1% Gd concentration [63]. According to the latest Double Chooz data [54], the near detector collected 412k IBD signals over 587 days, while the far detector took data of 125k IBD signals over 1276 days. We intend to utilize all data in analysis to examine new physics. The energy binning for ND and FD is identical, with the positron events divided into 38 bins in the energy range [1.0, 20.0] MeV.

3.2 RENO experiment

The full name of the RENO experiment is the Reactor Experiment for Neutrino Oscillation, located near the Hanbit Nuclear Power Plant in Korea yielding a total thermal power of 6×2.8 GW_{th}. RENO employed a dual detector design similar to that of Double Chooz, with two detectors located approximately 300 m and 1400 m from the reactors, respectively. The far detector of RENO was placed at $\phi = 39.2^\circ$ to the southeast of the reactors, with a co-latitude of $\chi = 54.6^\circ$, resulting in $\theta^{\text{LIV}} = 2.25$ rad.

The neutrino target of the RENO detector is similar in material to that of the Double Chooz, consisting of 16.5 tons of hydrocarbon LS mixed with 0.1% Gd concentration [64]. Our simulation analyzes about 120k IBD signal data from the far detector over approximately 2900 days until 2022, and includes around 990k data from the near detector over about 2500 days [55, 62], which are divided into 57 bins in the range [1.2, 8.4] MeV. We investigate neutrino oscillation by the data from the far detector divided into 45 bins in the energy range [1.2, 8.0] MeV.

Table 1 Summary of reactor neutrino experimental configurations

Experiment	Double Chooz		RENO		Daya Bay		
	ND	FD	ND	FD	EH1	EH2	EH3
Source	France		Korea		China		
Power [GW _{th}]	4.25 × 2		2.8 × 6		2.9 × 6		
LS mass	10.6 t	10.6 t	15.4 t	15.4 t	40.0 t	40.0 t	80.0 t
Baseline	400 m	1050 m	300 m	1400 m	512 m	561 m	1579 m
Data source	Ref. [54]		Refs. [55, 62]		Ref. [43]		
θ^{LIV}	1.86		2.25		0.74		

3.3 Daya Bay experiment

Daya Bay experiment is near the Daya Bay Nuclear Power Plant. There are three pairs of reactors, each with a power of 2.9 GW_{th}. The reactor neutrino experiments took a further step by placing detectors in three different orientations. The three experimental halls EH1, EH2, and EH3, were arranged with a baseline of 512 m, 561 m, and 1579 m from the reactor cores, respectively [65]. The farthest EH3 was located at the northwest of the reactor with $\phi = 216.6^\circ$ at $\chi = 67.4^\circ$, from which the LIV-related angle is calculated to be $\theta_{\text{DayaBay}}^{\text{LIV}} = 0.74$ rad.

Analogous to the Double Chooz and RENO detectors, the core of the Daya Bay detectors consisted of 20 tons of LS with 0.1% Gd concentration. We reproduced the data in the simulation tool with approximately 2.2 million IBD rates allocated to EH1, 2.5 million to EH2, and 764k to EH3, respectively. The data samples are divided into 26 bins in the energy range [0.7, 12.0] MeV. In the analysis, all data from the three experimental halls are used to quantify the neutrino oscillation and its new physics potentials.

3.4 Statistical method

The data analysis is based on the likelihood method for each experiment with the χ^2 function defined as follows:

$$\chi_{\text{exp}}^2(\theta_{13}, \Delta m_{ee}^2, \Delta\gamma) = \min_{\{\xi\}} \left[\sum_i \left(\frac{(O_{i,d} - T_{i,d}(\{\xi\}))^2}{O_{i,d}} \right) + \sum_k \frac{\xi_k^2}{\sigma_k^2} \right], \quad (7)$$

where $O_{i,d}$ is the observed events for each detector in each experiment, while the subscript i iterates over all energy bins, as d represents different detectors. Theoretically predicted events $T_{i,d}$ are represented by $T_{i,d}^{\text{osc}}$ without oscillation, based on experimental configurations given in Table 1. Our simulations were carried out using GLoBES [56, 57], with anisotropic LIV effects implemented in its neutrino oscillation calculation engine, where $\sin^2 \theta_{12} = 0.304$ and $\Delta m_{21}^2 = 7.42 \times 10^{-5} \text{ eV}^2$ [66] are used as input to the fit. Additionally, due to the short baseline, the uncertainties of matter density and $\theta_{12}, \Delta m_{21}^2$ can be neglected.

Meanwhile, the systematic uncertainties are introduced with a set of nuisance parameters ξ by the pull method [67], where normalization and energy calibration errors are taken into account. The normalization errors include reactor neutrino flux, detection efficiency and energy scale uncertainties, and the energy calibration error refers to the precision of neutrino energy reconstruction. These systematic errors are implemented via AEDL rule definitions in GLoBES [68], while the values of the systematical uncertainties σ_k are adopted from Refs. [41–43].

In total, 12 LIV parameters are tested sequentially in terms of both Standard Goodness-of-fit (SG) and Parameter Goodness-of-fit (PG) [44, 66]. SG is evaluated by the total χ^2 ,

$$\chi_{\text{SG}}^2 = \chi_{\text{Double Chooz}}^2 + \chi_{\text{RENO}}^2 + \chi_{\text{Daya Bay}}^2. \quad (8)$$

$\chi_{\text{SG,SM}}^2$ corresponding to standard neutrino oscillations is a special case with the LIV parameter $\Delta\gamma = 0$. Thus, we can test an extended LIV term by

$$\Delta\chi_{\text{SG}}^2 = \chi_{\text{SG,SM}}^2 - \chi_{\text{SG}}^2, \quad (9)$$

asymptotically following a chi-square function with one degree of freedom. It is noteworthy that we have fixed $\Delta m_{ee}^2 = 2.519 \times 10^{-3} \text{ eV}^2$ in χ^2 of the Double Chooz, since it only provided a precise measurement of $\sin^2(2\theta_{13})$ in the reference [41]. On the other hand, we have PG by

$$\chi_{\text{PG}}^2(\theta_{13}, \Delta m_{ee}^2, \Delta\gamma_{\text{LIV}}) = \chi_{\text{SG}}^2 - \sum_r^{\text{exp}} \chi_{r,\text{min}}^2. \quad (10)$$

$\chi_{r,\text{min}}^2$ is the minimum with the data only from a single experiment, while χ_{SG}^2 is involved with all three experiments. The p -value associated with the χ_{PG}^2 in statistics can be calculated for both the standard neutrino oscillation and the LIV scenario, taking into account their respective degrees of freedom (3 and 5).

By computing $\Delta\chi_{\text{SG}}^2$, we evaluate the extent to which introducing a LIV parameter improves the global fit of the theoretical prediction confronted with the combined experimental results. However, given that the three reactor experiments exhibit distinct sensitivities to LIV due to their different configurations represented by θ^{LIV} , the

Table 2 Fit results by minimizing χ_{SG}^2 and χ_{PG}^2 with each anisotropic LIV parameter. χ_{PG}^2 is characterized by 3 d.o.f. in standard neutrino oscillation and 5 d.o.f. under the LIV scenario.

Parameter	LIV value	$\sin^2(2\theta_{13})$	$\Delta m_{ee}^2 (10^{-3} \text{eV}^2)$	$\Delta\chi_{\text{SG}}^2$	χ_{PG}^2	p -value
SM	–	0.0873	2.535	–	5.55	0.14
$\mathcal{A}_{21}^{S(0)}$	1.17×10^{-17} MeV	0.0889	2.503	0.23	6.37	0.27
$\mathcal{A}_{21}^{S(1)}$	-3.34×10^{-18}	0.0889	2.511	0.77	5.95	0.31
$\mathcal{A}_{21}^{C(0)}$	-7.44×10^{-20} MeV	0.0873	2.536	$\simeq 0$	6.61	0.25
$\mathcal{A}_{21}^{C(1)}$	-2.69×10^{-18}	0.0880	2.518	0.62	6.29	0.28
\mathcal{B}_{21}^S	-2.21×10^{-18}	0.0880	2.516	0.78	6.13	0.29
\mathcal{B}_{21}^C	-2.92×10^{-17}	0.0874	2.533	0.17	6.74	0.24
$\mathcal{A}_{31}^{S(0)}$	-1.88×10^{-17} MeV	0.0877	2.459	1.00	6.53	0.26
$\mathcal{A}_{31}^{S(1)}$	7.70×10^{-19}	0.0875	2.525	0.10	6.77	0.24
$\mathcal{A}_{31}^{C(0)}$	2.43×10^{-17} MeV	0.0866	2.621	3.67	3.87	0.57
$\mathcal{A}_{31}^{C(1)}$	-3.44×10^{-18}	0.0866	2.572	2.06	4.82	0.44
\mathcal{B}_{31}^S	-2.50×10^{-17}	0.0866	2.570	2.16	4.72	0.45
\mathcal{B}_{31}^C	-3.00×10^{-17}	0.0873	2.538	0.20	6.68	0.25

statistic measure χ_{PG}^2 becomes essential to rigorously assess the inter-experiment consistency of the LIV parameters. Our analysis aims to demonstrate that the LIV-modified oscillation framework not only provides a superior phenomenological description of data but also fulfills the universality requirement across reactor experiments, thereby supporting its validity as a generalized extension in new physics searches.

4 Numerical results

In this work, we investigate the effect of the anisotropic LIV in the leading-order perturbation without a loss of generality. Numerical results based on $\Delta\chi_{\text{SG}}^2$ and χ_{PG}^2 are presented in light of 12 anisotropic LIV parameters, which can be sequentially examined. It is essential to check whether LIV can accommodate the tension between different experiments and improve the global fit to data in three reactor neutrino oscillation experiments. SG are PG complementary to examine the impact of LIV parameters, while the best-fit points in χ_{SG}^2 and χ_{PG}^2 are identical. The fit results of $\sin^2(2\theta_{13})$, Δm_{ee}^2 and the corresponding LIV values are presented in Table 2.

For χ_{SG}^2 , LIV parameters $\mathcal{A}_{31}^{S(0)}$, $\mathcal{A}_{31}^{C(0)}$, $\mathcal{A}_{31}^{C(1)}$ and \mathcal{B}_{31}^S exhibit an enhancement beyond 1σ , with $\mathcal{A}_{31}^{C(0)}$, $\mathcal{A}_{31}^{C(1)}$ and \mathcal{B}_{31}^S to demonstrate more pronounced effects, while $\mathcal{A}_{31}^{S(0)}$ yields the largest enhancement of about 1.9σ confidence level (C.L.) in standard goodness of fit. The anisotropic LIV parameters cause very little shift in the fitting results of $\sin^2(2\theta_{13})$ and Δm_{ee}^2 , where their impact is represented by $\mathcal{A}_{31}^{C(0)} = 2.43 \times 10^{-17}$ MeV shown in Fig. 2.

When it comes to χ_{PG}^2 , we have p -value to quantify PG before and after an introduction of each LIV param-

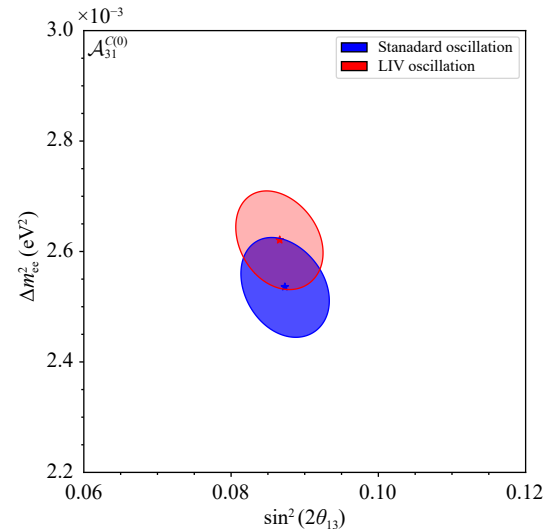


Fig. 2 Shifts of neutrino oscillation parameters under LIV effects. The red and blue correspond to the 90% C.L. analysis results of standard neutrino oscillation and LIV oscillation respectively, assuming normal mass hierarchy.

eter. In the standard neutrino oscillation framework, χ_{PG}^2 is characterized by three degrees of freedom, whereas in LIV scenario, it extends to five degrees of freedom. Bearing an increase of degrees of freedom in mind, we focus on the LIV parameters $\mathcal{A}_{31}^{C(0)}$, $\mathcal{A}_{31}^{C(1)}$ and \mathcal{B}_{31}^S that demonstrate the most significant improvements. When adopting $\alpha = 0.1$ as the compatibility threshold, the standard neutrino oscillation with $p = 0.14$ barely satisfies the threshold requirement, while the LIV framework with $\mathcal{A}_{31}^{C(0)}$ achieves high confidence level at $p = 0.57$. The consistency across experimental data samples from short-baseline reactor neutrino experiments is improved

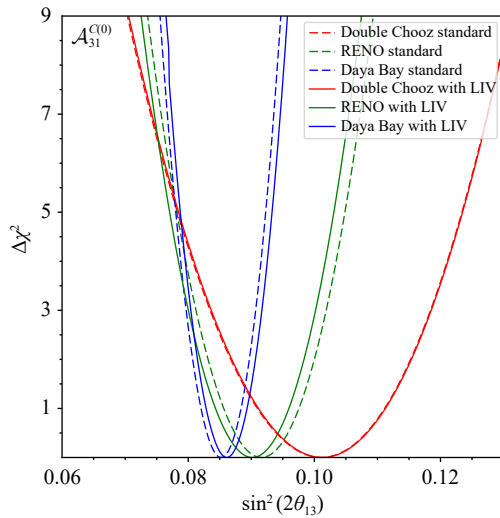


Fig. 3 χ^2 curves for $\sin^2(2\theta_{13})$ analysis of each experiment after introducing the LIV parameter $\mathcal{A}_{31}^{C(0)} = 2.43 \times 10^{-17}$ MeV. The red, green, and blue colors correspond to the Double Chooz, RENO, and Daya Bay experiments, respectively. The solid lines represent the χ^2 curves under the effect of LIV, while the dashed lines are in the standard neutrino oscillation case. Δm_{ee}^2 is fixed at $2.519 \times 10^{-3} \text{ eV}^2$, assuming normal mass hierarchy.

significantly, as shown in Figs. 3 and 4. The fit results of RENO and Daya Bay tend to unify, while the result of Double Chooz is almost the same as the result given by the standard neutrino oscillation. Due to the coupling between \mathcal{A}_C and $\cos\theta^{\text{LIV}}$, Double Chooz remains relatively insensitive to LIV effects since its θ^{LIV} is close to $\pi/2$. In contrast, RENO and Daya Bay each exhibit appreciable $\cos\theta^{\text{LIV}}$ value with opposite signs, leading to antithetical LIV effects that help reconcile the discrepancies among the results.

The best-fit LIV parameters in $\Delta\gamma$ are almost at the same order consistent with the previous experimental limits [69], including those published by the reactor neutrino experiments Daya Bay [36] and Double Chooz [37].

5 Conclusion

Lorentz invariance violation has profound impacts on the data analysis and physics interpretation in the laboratory frame, which may not only lead to periodic variations in the reactor neutrino survival probability but also induce discrepancies between the results of different experiments. In the present work, the latest data from short-baseline reactor neutrino experiments were used to explore the effects of anisotropic LIV. We analysed dataset from Double Chooz, RENO, and Daya Bay by incorporating the LIV mechanism into the mass eigenstates of neutrinos.

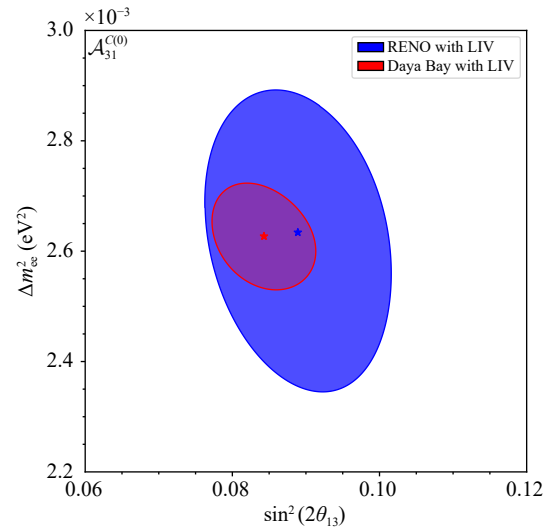


Fig. 4 90% C.L. space of neutrino oscillation parameters for the RENO and Daya Bay experiments after introducing $\mathcal{A}_{31}^{C(0)} = 2.43 \times 10^{-17}$ MeV. The red and blue colors represent the results of Daya Bay and RENO, respectively. The star markers indicate the best-fit points, assuming normal neutrino mass hierarchy. Double Chooz is excluded owing to its absence of a precise Δm_{ee}^2 measurement [41].

Our results indicated that anisotropic LIV model provides a better fit to the total data with respect to standard neutrino oscillation up to 1.9σ C.L., with $\mathcal{A}_{31}^{C(0)} = 2.43 \times 10^{-17}$ MeV, $\sin^2(2\theta_{13}) = 0.0866$, $\Delta m_{ee}^2 = 2.621 \times 10^{-3} \text{ eV}^2$ yielding the best-fit. Meanwhile, the LIV $\mathcal{A}_{31}^{C(0)}$ demonstrated the best parameter goodness-of-fit, resolving the tension between short-baseline reactor neutrino experiments data ($p_{\text{PG}} = 0.57$), whereas the standard neutrino oscillation fit remains proximity to the tension boundary ($p_{\text{PG}} = 0.14$) with an acceptance criterion of $\alpha = 0.1$. The inclusion of LIV effects caused minimal changes to the best-fit values of $\sin^2(2\theta_{13})$ and Δm_{ee}^2 for the overall dataset, while the results from RENO and Daya Bay show convergence.

We anticipate that the next-generation neutrino oscillation experiments like Jiangmen Underground Neutrino Observatory (JUNO) [70] will be able to examine such LIV effects soon.

6 Note added

During the editing process, the updated results from the RENO experiment [71] indicate observable deviations from the dataset utilized in this analysis. While the conclusions derived from the data released by the RENO experiment until 2020 [55] remain valid, the newly reported measurements suggest a mitigated sensitivity to the anisotropic LIV effect.



Declarations The authors declare that they have no competing interests and there are no conflicts.

Acknowledgements This project was supported in part by the National Natural Science Foundation of China under Grant No. 12347105. This work was supported in part by the Fundamental Research Funds for the Central Universities (No. 23xkjc017) in Sun Yat-sen University. J.T. is grateful to Southern Center for Nuclear-Science Theory (SCNT) at Institute of Modern Physics in Chinese Academy of Sciences for hospitality. We appreciate Sampsa Vihonen's early-stage involvement in the project and extend gratitude to Yinyuan Huang for his coding contributions.

Appendix A: The relation between SME coefficients and effective anisotropic LIV parameters

In the leading-order perturbative expansion approximation, the effective Hamiltonian with SME coefficients can be written as

$$(\mathcal{H}_{\text{LIV}})_{ij} = \frac{\delta_{ij}}{E} (a_L^\mu p_\mu - c_L^{\mu\nu} p_\mu p_\nu)_{ij}, \quad (\text{A1})$$

$i, j = 1, 2, 3$ correspond to different mass states of neutrinos. The LIV coefficients in mass eigenstates have a linear correspondence with the coefficients in Eq. (2),

$$\begin{aligned} (a_L^\mu)_{ij} &= U_{i\alpha} (a^\mu + b^\mu)_{\alpha\beta} (U^\dagger)_{\beta j}, \\ (c_L^{\mu\nu})_{ij} &= U_{i\alpha} (c^{\mu\nu} + d^{\mu\nu})_{\alpha\beta} (U^\dagger)_{\beta j}. \end{aligned} \quad (\text{A2})$$

We assume that the mass states of neutrinos during propagation are physical states, without mixing effects between mass states. Diagonal elements of the Hamiltonian are real numbers required by hermiticity. Therefore, a_{ij} and c_{ij} can be regarded as 3×3 diagonal real matrices, with mass dimensions of 1 and 0, respectively. For antineutrinos, $a_L \rightarrow -a_L$.

As mentioned in Eq. (4), the Hamiltonian term causing anisotropic LIV can be reconstructed into a form dependent on directional factors,

$$\begin{aligned} (\mathcal{H}_{\text{LIV}})_{ij} &= \{a_L^X \cos(\omega t) + a_L^Y \sin(\omega t) - 2[c_L^{TX} \cos(\omega t) \\ &\quad + c_L^{TY} \sin(\omega t)]E\} \sin\theta^{\text{LIV}} + (a_L^Z - 2c_L^{TZ}E) \cos\theta^{\text{LIV}} \\ &\quad - [c_L^{XZ} \cos(\omega t) + c_L^{YZ} \sin(\omega t)]E \sin(2\theta^{\text{LIV}}) \\ &\quad + \frac{1}{2} \left[\left(-c_L^{ZZ} + \frac{1}{2}c_L^{XX} + \frac{1}{2}c_L^{YY} \right) \right. \\ &\quad + \frac{1}{2}(c_L^{XX} - c_L^{YY}) \cos(2\omega t) \\ &\quad \left. + c_L^{XY} \sin(2\omega t) \right] E \cos(2\theta^{\text{LIV}}). \end{aligned} \quad (\text{A3})$$

Here, θ^{LIV} is the same as that in Eq. (4), and $\phi^{\text{LIV}} = \omega t$ corresponds to the azimuthal angle in the XY plane of this Sun-center reference frame, while the zenith angle is

approximated as $\pi/2$. Following the form of mass-squared differences term in standard neutrino oscillation Hamiltonian, the effective LIV Hamiltonian can be expressed as

$$\begin{aligned} \mathcal{H}_{\text{LIV}}^{\text{eff}} &= \text{Diagonal}(0, \Delta\gamma_{21}, \Delta\gamma_{31}), \\ \Delta\gamma_{ij} &= \frac{1}{E} [(a_L^\mu p_\mu - c_L^{\mu\nu} p_\mu p_\nu)_{ii} - (a_L^\mu p_\mu - c_L^{\mu\nu} p_\mu p_\nu)_{jj}]. \end{aligned} \quad (\text{A4})$$

This expression is equivalent to Eq. (A1) for neutrino oscillations. In neutrino experiments conducted over several years, the effects of the azimuthal angle ϕ^{LIV} can be represented by the mean value of the periodic function, retaining only the directional dependence on the polar angle θ^{LIV} . After integration, the general form of the anisotropic LIV Hamiltonian in Eq. (4) can be obtained,

$$\Delta\gamma(a^\mu, c^{\mu\nu}) \rightarrow \Delta\gamma(\mathcal{A}, \mathcal{B}).$$

The neutrino oscillation probability calculated from the former is a periodic function dependent on sidereal time, while the oscillation probability calculated from the latter equals the average value of this periodic function,

$$P(\mathcal{A}, \mathcal{B}) \simeq \frac{1}{T} \int_0^T P_{\bar{\nu}_e \rightarrow \bar{\nu}_e}(a_L^\mu, c_L^{\mu\nu}, t) dt. \quad (\text{A5})$$

The neutrino beam traverses all azimuths in $T = 2\pi/\omega = 23 \text{ h } 56 \text{ min}$ due to the Earth's rotation.

References and notes

1. P. A. Zyla, et al. (Particle Data Group), Review of particle physics, *Prog. Theo. Exp. Phys.* 2020(8), 083C01 (2020)
2. V. Barger, D. Marfatia, and K. L. Whisnant, *The Physics of Neutrinos*, Princeton University Press, Princeton, 2012
3. R. Mohapatra and P. Pal, *Massive Neutrinos in Physics and Astrophysics*, Cambridge University Press, 1992
4. P. Langacker, Grand unified theories and proton decay, *Phys. Rep.* 72(4), 185 (1981)
5. V. A. Kostelecký and R. Potting, Gravity from spontaneous Lorentz violation, *Phys. Rev. D* 79(6), 065018 (2009)
6. M. D. C. Torri and L. Miramonti, Neutrinos as possible probes for quantum gravity, arXiv: 2404.04076 [gr-qc] (2025)
7. V. A. Kostelecký and S. Samuel, Spontaneous breaking of Lorentz symmetry in string theory, *Phys. Rev. D* 39(2), 683 (1989)
8. V. Alan Kostelecký and R. Potting, CPT and strings, *Nucl. Phys. B* 359(2-3), 545 (1991)
9. M. S. Berger and V. A. Kostelecký, Supersymmetry and Lorentz violation, *Phys. Rev. D* 65(9), 091701 (2002)
10. O. W. Greenberg, CPT violation implies violation of

- Lorentz invariance, *Phys. Rev. Lett.* 89(23), 231602 (2002)
11. J. S. Schwinger, The theory of quantized fields. I, *Phys. Rev.* 82(6), 914 (1951)
 12. G. Lüders, Proof of the TCP theorem, *Ann. Phys.* 2(1), 1 (1957)
 13. V. Antonelli, L. Miramonti, and M. D. C. Torri, Phenomenological effects of CPT and Lorentz invariance violation in particle and astroparticle physics, *Symmetry (Basel)* 12(11), 1821 (2020)
 14. R. Cordero, L. A. Delgado, O. G. Miranda, and C. A. Moura, Neutrino Lorentz invariance violation from the CPT-even SME coefficients through a tensor interaction with cosmological scalar fields, *Eur. Phys. J. C* 85(1), 6 (2025)
 15. Y. Huang and B. Q. Ma, Ultra-high energy cosmic neutrinos from gamma-ray bursts, *Fundamental Res.* 4(1), 51 (2024)
 16. I. Collaboration, et al., A search for extremely-high-energy neutrinos and first constraints on the ultra-high-energy cosmic-ray proton fraction with IceCube, arXiv: 2502.01963 [astro-ph.HE] (2025)
 17. Y. M. Yang, X. J. Lv, X. J. Bi, and P. F. Yin, Constraints on Lorentz invariance violation in neutrino sector from the ultra-high-energy event km³-230213a, arXiv: 2502.18256 [hep-ph] (2025)
 18. M. D. C. Torri, Neutrino oscillations and Lorentz invariance violation, *Universe* 6(3), 37 (2020)
 19. D. Colladay and V. A. Kostelecky, CPT violation and the standard model, *Phys. Rev. D* 55(11), 6760 (1997)
 20. D. Colladay and V. A. Kostelecky, Lorentz-violating extension of the standard model, *Phys. Rev. D* 58(11), 116002 (1998)
 21. V. A. Kostelecký, Gravity, Lorentz violation, and the standard model, *Phys. Rev. D* 69(10), 105009 (2004)
 22. P. Adamson, et al. (MINOS Collaboration), Search for Lorentz invariance and CPT violation with the MINOS far detector, *Phys. Rev. Lett.* 105, 151601 (2010)
 23. P. Adamson, et al. (MINOS Collaboration), Testing Lorentz invariance and CPT conservation with NuMI neutrinos in the MINOS near detector, *Phys. Rev. Lett.* 101, 151601 (2008)
 24. P. Adamson, et al. (The MINOS Collaboration), Search for Lorentz invariance and C P T violation with muon antineutrinos in the MINOS Near Detector, *Phys. Rev. D* 85, 031101 (2012)
 25. L. B. Auerbach, et al. (LSND Collaboration), Tests of Lorentz violation in $\bar{\nu}_\mu \rightarrow \bar{\nu}_e$ oscillations, *Phys. Rev. D* 72, 076004 (2005)
 26. S. Sahoo, A. Kumar, and S. K. Agarwalla, Probing Lorentz Invariance Violation with atmospheric neutrinos at INO-ICAL, *J. High Energy Phys.* 2022(3), 50 (2022)
 27. S. Sahoo, A. Kumar, S. K. Agarwalla, and A. Dighe, Discriminating between Lorentz violation and non-standard interactions using core-passing atmospheric neutrinos at INO-ICAL, *Phys. Lett. B* 841, 137949 (2023)
 28. D. Raikwal, S. Choubey, and M. Ghosh, Comprehensive study of Lorentz invariance violation in atmospheric and long-baseline experiments, *Phys. Rev. D* 107(11), 115032 (2023)
 29. R. Abbasi, et al. (IceCube Collaboration), Test of Lorentz invariance with atmospheric neutrinos, *Phys. Rev. D* 82, 112003 (2010)
 30. K. Abe, et al. (Super-Kamiokande Collaboration), Test of Lorentz invariance with atmospheric neutrinos, *Phys. Rev. D* 91, 052003 (2015)
 31. K. Abe, et al. (T2K Collaboration), Search for Lorentz and CPT violation using sidereal time dependence of neutrino flavor transitions over a short baseline, *Phys. Rev. D* 95, 111101 (2017)
 32. S. K. Agarwalla, S. Das, S. Sahoo, and P. Swain, Constraining Lorentz invariance violation with next-generation long-baseline experiments, *J. High Energy Phys.* 2023(7), 216 (2023)
 33. S. Pan, K. Chakraborty, and S. Goswami, Sensitivity to CP discovery in the presence of Lorentz invariance-violating potential at T2HK/T2HKK, *Eur. Phys. J. C* 84(4), 354 (2024)
 34. S. Mishra, S. Shukla, L. Singh, and V. Singh, Search for Lorentz violations through the sidereal effect at the NO ν A experiment, *Phys. Rev. D* 109(7), 075042 (2024)
 35. A. Aguilar-Arevalo, C. Anderson, A. Bazarko, S. Brice, B. Brown, et al., Test of Lorentz and CPT violation with short baseline neutrino oscillation excesses, *Phys. Lett. B* 718(4–5), 1303 (2013)
 36. D. Adey, et al. (Daya Bay Collaboration), Search for a time-varying electron antineutrino signal at Daya Bay, *Phys. Rev. D* 98, 092013 (2018)
 37. Y. Abe, et al. (Double Chooz Collaboration), First test of Lorentz violation with a reactor-based antineutrino experiment, *Phys. Rev. D* 86, 112009 (2012)
 38. Y. F. Li and Z. Zhao, Tests of Lorentz and CPT violation in the medium baseline reactor antineutrino experiment, *Phys. Rev. D* 90(11), 113014 (2014)
 39. A. Sarker, A. Medhi, and M. M. Devi, Investigating the effects of Lorentz invariance violation on the CP-sensitivities of the deep underground neutrino experiment, *Eur. Phys. J. C* 83(7), 592 (2023)
 40. S. Mishra, S. Shukla, L. Singh, and V. Singh, Exploring non-isotropic Lorentz invariance violation through sidereal effect at dune, arXiv: 2410.09248 [hep-ph] (2024)
 41. H. de Kerret, et al. (Double Chooz Collaboration), Double Chooz θ_{13} measurement via total neutron capture detection, *Nat. Phys.* 16, 558 (2020)
 42. G. Bak, et al. (RENO Collaboration), Measurement of reactor antineutrino oscillation amplitude and frequency at RENO, *Phys. Rev. Lett.* 121, 201801 (2018)
 43. F. P. An, et al. (Daya Bay Collaboration), Precision measurement of reactor antineutrino oscillation at kilometer-scale baselines by Daya Bay, *Phys. Rev. Lett.* 130, 161802 (2023)
 44. M. Maltoni and T. Schwetz, Testing the statistical compatibility of independent data sets, *Phys. Rev. D* 68(3), 033020 (2003)
 45. V. A. Kostelecky and M. Mewes, Lorentz and CPT violation in neutrinos, *Phys. Rev. D* 69, 016005 (2004)
 46. V. A. Kostelecky and M. Mewes, Lorentz violation and short-baseline neutrino experiments, *Phys. Rev. D* 70(7), 076002 (2004)
 47. M. Aker, et al. (KATRIN), Direct neutrino-mass measurement with sub-electronvolt sensitivity, *Nat. Phys.* 18, 160 (2022)

48. S. Coleman and S. L. Glashow, High-energy tests of Lorentz invariance, *Phys. Rev. D* 59(11), 116008 (1999)
49. A. Addazi, J. Alvarez-Muniz, R. A. Batista, G. Amelino-Camelia, V. Antonelli, et al., Quantum gravity phenomenology at the dawn of the multi-messenger era — A review, *Prog. Part. Nucl. Phys.* 125, 103948 (2022)
50. V. A. Kostelecký and M. Mewes, Lorentz and CPT violation in the neutrino sector, *Phys. Rev. D* 70(3), 031902 (2004)
51. A. Kostelecky and M. Mewes, Neutrinos with Lorentz-violating operators of arbitrary dimension, *Phys. Rev. D* 85(9), 096005 (2012)
52. J. Kopp, M. Lindner, T. Ota, and J. Sato, Nonstandard neutrino interactions in reactor and superbeam experiments, *Phys. Rev. D* 77(1), 013007 (2008)
53. B. Pontecorvo, Neutrino experiments and the problem of conservation of leptonic charge, *Zh. Eksp. Teor. Fiz.* 53, 1717 (1967)
54. P. Soldin (Double Chooz Collaboration), Precision neutrino mixing angle measurement with the Double Chooz experiment and latest results, *PoS TAU* 228, 2023 (2024)
55. C. Shin (RENO), Recent results from RENO, *PoS ICHE* 177, 2020 (2021)
56. P. Huber, M. Lindner, and W. Winter, Simulation of long-baseline neutrino oscillation experiments with GLoBES, *Comput. Phys. Commun.* 167(3), 195 (2005)
57. P. Huber, J. Kopp, M. Lindner, M. Rolinec, and W. Winter, New features in the simulation of neutrino oscillation experiments with GLoBES 3.0, *Comput. Phys. Commun.* 177(5), 432 (2007)
58. F. P. An, et al. (Daya Bay Collaboration), Measurement of the reactor antineutrino flux and spectrum at Daya Bay, *Phys. Rev. Lett.* 116, 061801 (2016)
59. J. M. Berryman and P. Huber, Sterile neutrinos and the global reactor antineutrino dataset, *J. High Energy Phys.* 2021(1), 167 (2021)
60. The geographic information for each experiment was partially referenced from Google Maps results.
61. H. X. Lin, Reactor neutrino liv phenomenology toolkit, URL: github.com/Star-Leaf777/LIV-reactors-linhx (2023)
62. K. K. Joo, Reactor Neutrino I_Results of reactor antineutrinos at RENO, doi: 10.5281/zenodo.6683722 (2022)
63. H. de Kerret, Y. Abe, C. Aberle, T. Abrahão, J. M. Ahijado, et al., The Double Chooz antineutrino detectors, *Eur. Phys. J. C* 82(9), 804 (2022)
64. S. H. Seo, et al. (RENO Collaboration), Spectral measurement of the electron antineutrino oscillation amplitude and frequency using 500 live days of RENO data, *Phys. Rev. D* 98, 012002 (2018)
65. F. P. An, et al. (Daya Bay Collaboration), Spectral measurement of electron antineutrino oscillation amplitude and frequency at Daya Bay, *Phys. Rev. Lett.* 112, 061801 (2014)
66. I. Esteban, M. Gonzalez-Garcia, M. Maltoni, T. Schwetz, and A. Zhou, The fate of hints: updated global analysis of three-flavor neutrino oscillations, *J. High Energy Phys.* 2020(9), 178 (2020)
67. G. L. Fogli, E. Lisi, A. Marrone, D. Montanino, and A. Palazzo, Getting the most from the statistical analysis of solar neutrino oscillations, *Phys. Rev. D* 66(5), 053010 (2002)
68. P. Huber, J. Kopp, M. Lindner, and W. Winter, GLoBES User's and Experiment Definition Manual, Heidelberg, Germany; Blacksburg, VA, USA; Geneva, Switzerland; Zeuthen, Germany, Version 3.2.18 (May 5, 2020)
69. V. A. Kostelecký and N. Russell, Data tables for Lorentz and CPT violation, *Rev. Mod. Phys.* 83(1), 11 (2011)
70. A. Abusleme, et al. (JUNO), JUNO physics and detector, *Prog. Part. Nucl. Phys.* 123, 103927 (2022), arXiv: 2104.02565 [hep-ex]
71. S. Jeon, et al., Measurement of reactor antineutrino oscillation amplitude and frequency using 3800 days of complete data sample of the reno experiment, arXiv: 2412.18711 [hep-ex] (2024)